Current Optics and Photonics
Vol. 3, No. 6, December 2019, pp. 541-547

ISSN: 2508-7266(Print) / ISSN: 2508-7274(Online)
DOI: https://doi.org/10.3807/COPP.2019.3.6.541

A Novel Photonic Crystal Fiber Sensor with Three D-shaped Holes Based on Surface Plasmon Resonance

Pibin Bing[1]*, Jialei Sui[1], Shichao Huang[1], Xinyue Guo[1], Zhongyang Li[1], Lian Tan[1], and Jianquan Yao[1,2]

[1]College of Electric Power, North China University of Water Resources and Electric Power, Zhengzhou 450045, China
[2]College of Precision Instrument and Opto-electronics Engineering, Institute of Laser and Opto-electronics, Tianjin University, Tianjin, 300072, China

(Received May 20, 2019 : revised August 7, 2019 : accepted September 28, 2019)

A novel photonic crystal fiber (PCF) sensor with three D-shaped holes based on surface plasmon resonance (SPR) is analyzed in this paper. Three D-shaped holes are filled with the analyte, and the gold film is deposited on the side of three planes. The design of D-shaped holes with outward expansion can effectively solve the uniformity problem of metallized nano-coating, it is beneficial to the filling of the analyte and is convenient for real-time measurement of the analyte. Compared with the hexagonal lattice structure, the triangular arrangement of the clad air holes can significantly reduce the transmission loss of light and improve the sensitivity of the sensor. The influences of the air hole diameter, the distance between D-shaped holes and core, and the counterclockwise rotation angle of D-shaped holes on sensing performance are studied. The simulation results show that the wavelength sensitivity of the designed sensor can be as high as 10100 nm/RIU and the resolution can reach 9.9×10^{-6} RIU.

Keywords : Photonic crystal fiber, Wavelength sensitivity, Surface plasmon resonance
OCIS codes : (060.2370) Fiber optics sensors; (060.5295) Photonic crystal fibers; (240.6680) Surface plasmons

I. INTRODUCTION

When light is incident on the surface of a metal medium, surface plasmon resonance (SPR) occurs between the evanescent wave generated by total reflection and the excited surface plasmons under the condition of phase matching. The phenomenon is that the incident light with specific wavelength is absorbed and a significant absorption peak appears in the detection spectrum. The position of the absorption peak is very sensitive to the change of the refractive index (RI) of the analyte which can be converted to the offset variation of the resonance peak, so as to realize sensing [1]. In recent years, with the development of the prism SPR sensor, the fiber SPR sensor [2], the grating coupled SPR sensor [3] and the photonic crystal fiber (PCF) SPR sensor [4-6], SPR sensors have been widely used in sensing and monitoring. The PCF can reduce the RI of the fiber due to introduced holes, solving the problem of phase matching effectively [7]. Moreover, the PCF-SPR sensors do not need an additional coupling device, and they have advantages such as small size, high sensitivity, flexible design and the like. Because of flexibility in structure design, different PCF structures could have unique advantages when used as sensors. Sensors with multi-core [8] and liquid core [9] structure can detect high RI materials. For instance, the reported multi-core PCF sensor [8] can achieve RI detection in the range of 1.33 to 1.53, and the range of dual-core structure sensor [10] is 1.33 to 1.51. The slotted structure [11] and the D-shaped structure [12, 13] can reduce difficulty in coating and solve the problem of filling analyte. However, coating material plays a particularly important role in improving the performance of a sensor under the same PCF structure. Gold

*Corresponding author: bing463233@163.com, ORCID 0000-0003-0059-135X
Color versions of one or more of the figures in this paper are available online.

and silver are commonly used metal materials for coating, and the sensitivity and resolution of the silver-plated film are higher than those of the gold-plated film [14]. However, the silver becomes oxidized and thus leads to low detection accuracy. In order to solve the problem, researchers put forward the coating structures of gold-silver layer [15] and graphene-silver layer [16]. In addition, the setting of the coating position in the structural design is also an important factor affecting the sensing performance. The sensor with selective coating can reduce the coupling between adjacent surface plasmon polaritons (SPP) modes, which can increase the sensitivity [17].

In recent years, the PCF-SPR sensors have been widely used in the detection of temperature [18], magnetic field [19], and the RI. However, few PCF sensors can be commercialized and scaled in a short time due to the need for uniformity of the metal coating and the filling of the analyte in the tiny air holes, which severely limit the development and application of the PCF-SPR sensors.

A novel PCF sensor with three D-shaped holes is designed and simulated in this paper. The D-shaped holes can be expanded outward until the planes of D-shaped holes are exposed in the air, so it can adjust the size of the D-shaped expansion according to the actual requirement. When the planes of D-shaped holes are exposed in the air, the PCF can be immersed directly in the analyte for sensing, it can effectively solve the uniformity problem of the metal coating and facilitate the filling of the analyte at the same time. The effects of structural parameters on the sensing performance are studied. The numerical analyses indicate that the resonance peak shows a red shift and the wavelength sensitivity increases with the increasing of distance between the D-shaped holes and the core. The introduction of the central air hole can improve the wavelength sensitivity. The wavelength sensitivity of the sensor increases with the increasing of the rotation angle due to the deviation caused by the counterclockwise rotation of the D-shaped holes in the manufacturing.

II. DESIGN AND ANALYSIS

The 2D simulation of the PCF sensor we proposed is established and the mode characteristics are investigated by the FEM with the COMSOL Multiphysics software. Figure 1 represents the cross-section of the novel PCF sensor with three D-shaped holes. The air holes in the cladding layer are arranged in triangular lattice with a space of $\Lambda = 2$ μm, the diameter of which is $d_1 = 0.6\Lambda$, the diameter of the central air hole is $d_c = 0.2\Lambda$. Three D-shaped holes around the outside of the triangular lattice, and can be expanded outward until the planes of D-shaped holes are exposed in the air. In Fig. 1, the D-shaped hole has a radius of 4.5 μm and a vertical distance from the center of the optical fiber is $h = 3$ μm, and it is shifted to the right by 2 μm from the central axis. The dimensions of the three D-shaped

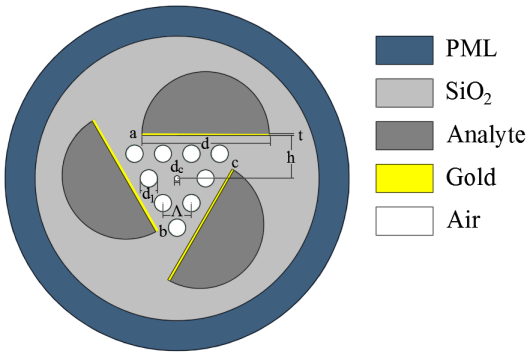

FIG. 1. Schematic of the designed sensor.

holes are the same, but the phase difference is 120 degrees in turn. The D-shaped holes' planes which are closed to the fiber core are coated with gold film, and the thickness of the gold film (t) is 40 nm. The dielectric constant of gold is given by the Drude model [20]. Deposition of metal layers inside of the PCF can be performed by a high pressure CVD technique or by a wet chemistry deposition technique used in fabrication [1]. The background material is SiO_2 whose RI is given by the Sellmeier equation [21]:

$$n_{SiO_2}^2(\lambda) = 1 + \frac{A_1\lambda^2}{\lambda^2 - B_1} + \frac{A_2\lambda^2}{\lambda^2 - B_2} + \frac{A_3\lambda^2}{\lambda^2 - B_3} \quad (1)$$

where λ represents the wavelength of incident light, and $A_1 = 0.696166300$, $A_2 = 0.407942600$, $A_3 = 0.897479400$, $B_1 = 4.67914826 \times 10^{-3}$ μm^2, $B_2 = 1.35120631 \times 10^{-2}$ μm^2, $B_3 = 97.9340025$ μm^2. Three D-shaped holes are filled with the analyte, and the RI of the analyte (n_a) varies in the range of 1.33 to 1.39.

The incident light with a certain wavelength is incident on the designed PCF sensor, the surface plasmons can be excited at the interface between the gold layer and the analyte. When the core-guided mode is phase-matched with the SPP mode, the surface plasmons resonate with the evanescent wave generated by total reflection. The phase matching point is the intersection of the effective RI of the core-guided mode and the SPP mode. As we all know, the real part of the effective RI of the core-guided mode is related to the transmission medium. The incident light transmits in the symmetrical core of PCF, and the real parts of the effective RIs of the core-guided mode have no significant difference in the x-polarization and y-polarization direction. The imaginary part of the effective RI is proportional to the transmission loss of PCF, which means it is strongly related to the tested analyte. The PCF we proposed is a rotationally symmetric structure. So, there is no significant difference in the imaginary part of the effective RIs of the core-guided mode between the two polarization directions. Therefore, the structure is polarization independent, the x-polarization direction is chosen for analysis.

When the surface plasmons resonate with the evanescent wave generated by total reflection, a significant absorption peak appears in the detected spectrum. Figure 2(a) is the electric field distribution of the core-guided mode at the resonance peak in the case of $n_a = 1.36$. The electric field intensity distribution from point p1 to point p2 is as shown in Fig. 2(b). It can be seen that part of the energy leakage into the interface between the metal and the analyte results in the SPR effect.

The PCF-SPR sensor achieves the measurement of analyte by detecting the shift of the resonance peak. According to Ref. [22], the loss is defined as:

$$\alpha_{loss}(dB/m) = 40\pi \,\mathrm{Im}[n_{eff}]/\ln(10)\lambda \tag{2}$$

where λ is the wavelength of the incident light, and n_{eff} is the effective RI of the core-guided mode. Figure 3(a) shows the change of resonant peak when n_a changes from 1.33 to 1.39. When the RI of the analyte (n_a) increases, the resonance intensity gradually increases and the formant has a redshift. And it happens due to the reduction of the RI contrast between the core-guided mode and SPP mode. Because of the small RI contrast, there is less light confinement through the core than light penetration through the cladding region, resulting in more light coupling with the metal surface and interacting with the analyte.

The important parameters for judging the performance of a sensor are sensitivity and resolution. In the wavelength interrogation mode, the change of the analyte RI is detected by measuring displacement of a resonance peak. In this case, wavelength sensitivity is defined as:

$$S_\lambda(nm/RIU) = \Delta\lambda_{peak}/\Delta n_a \tag{3}$$

where $\Delta\lambda_{peak}$ represents resonance peak shift and Δn_a represents the RI change of analyte. As shown in Fig. 3(b), when the RI of the analyte (n_a) changes from 1.38 to 1.39, the formant shift is the largest, $\Delta\lambda_{peak}$ is 101 nm, and thus

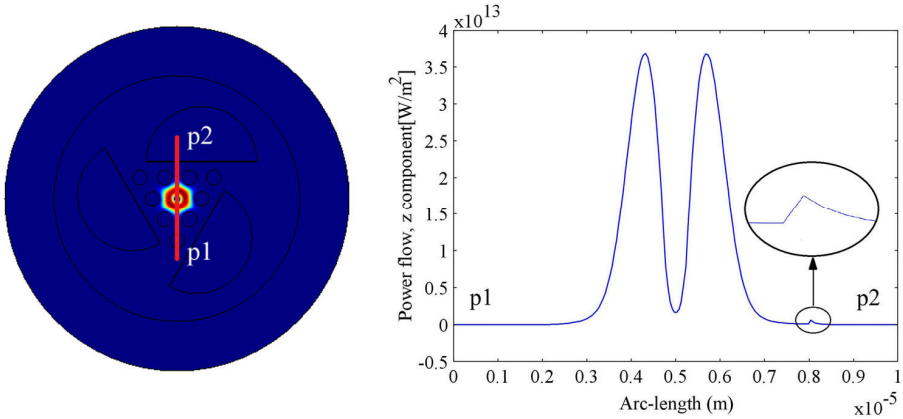

(a) (b)

FIG. 2. (a) The profile of core-guided mode at the resonant peak with $n_a = 1.36$; (b) The distribution of the electric field intensity from point p1 to point p2.

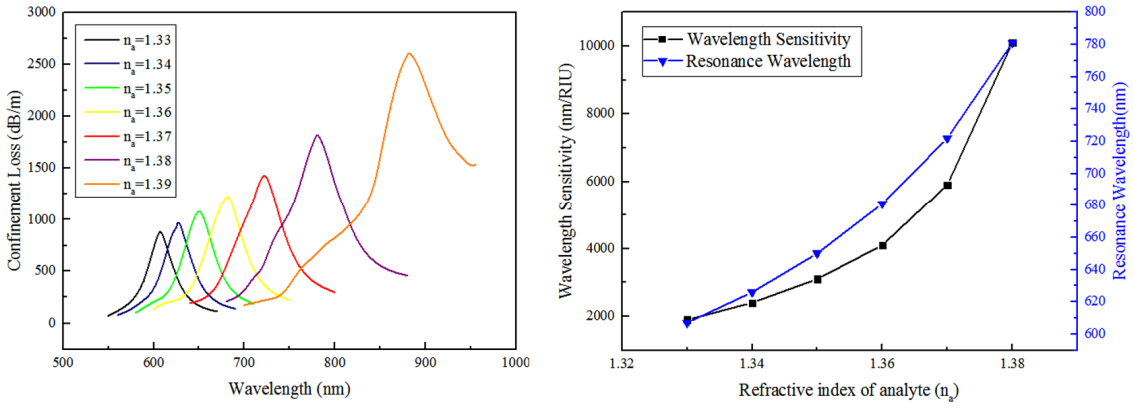

(a) (b)

FIG. 3. (a) Loss with the RI of analyte changing from 1.33 to 1.39; (b) The variation of wavelength sensitivity and resonance wavelength changing with RI of analyte.

the wavelength sensitivity S_λ is obtained to be as high as 10100 nm/RIU. The resolution is defined as [23]:

$$R(RIU) = \Delta\lambda_{\min}\Delta n / \Delta\lambda_{res} = \Delta\lambda_{\min} / S_\lambda \quad (4)$$

where $\Delta\lambda_{min}$ is the minimum resolution of the spectrum. Assuming that the minimum unit of spectrometer resolution ($\Delta\lambda_{min}$) is 0.1 nm, the resolution of the designed sensor is 9.9×10^{-6} RIU according to the Eq. (4).

III. RESULTS AND DISCUSSION

In this novel PCF sensor, the D-shape holes can be expanded outward until the planes of D-shaped holes are exposed in the air, Ref. [24] has pointed out that the design depends neither on the refractive indices nor on the absolute physical dimensions of the fiber, so that the design can be scalable. And the wavelength sensitivity can be affected by the gold layer in Ref. [21]. So the D-shape holes can be expanded outward as long as the distance between the fiber core and gold film is fixed. The D-shape holes' size has less influence on the resonance wavelength in that equal amount of light is coupled to the metal surface no matter what the size is. Therefore, when the planes of D-shaped holes are exposed in the air, they do not need to be coated in the air holes. This can effectively solve the problem of coating. As shown in Fig. 4, the clad air holes which are arranged in a triangular lattice lead to the lower RI of the cladding. This, in turn, increases the core-cladding RI contrast, hence increasing modal confinement in the core region, and resulting in lower modal losses due to coupling to a metal surface in the second layer. The variation of analyte RI is the same, the triangular arrangement is more sensitive. Therefore, cladding air holes in triangular arrangement structure can significantly reduce the transmission loss of light and improve the sensitivity of the sensor.

The size of the central air hole has a direct impact on the sensitivity of the sensor. The change of resonance peak is shown in Fig. 5(a), when the RI of analyte (n_a) is 1.37

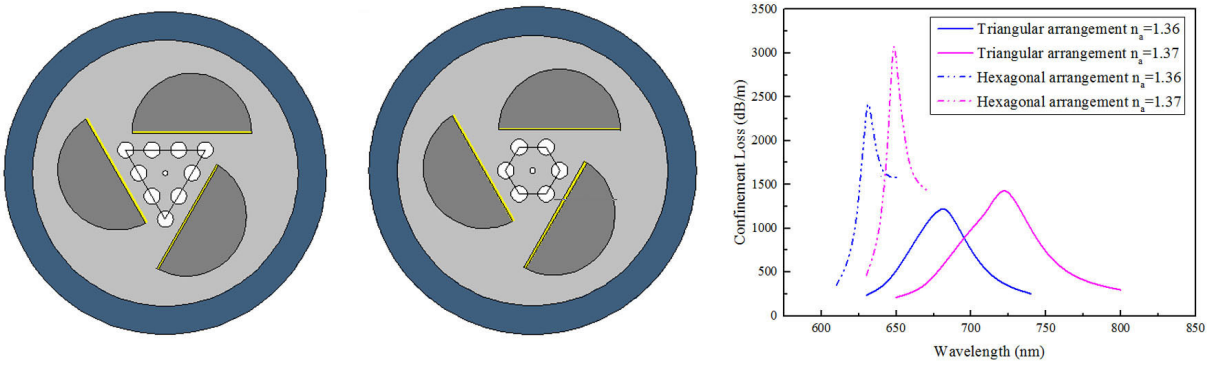

(a) (b) (c)

FIG. 4. (a) Air holes in triangular arrangement structure; (b) Air holes in hexagonal arrangement structure; (c) Loss comparison between triangular arrangement and hexagonal arrangement with $n_a = 1.36$ and $n_a = 1.37$.

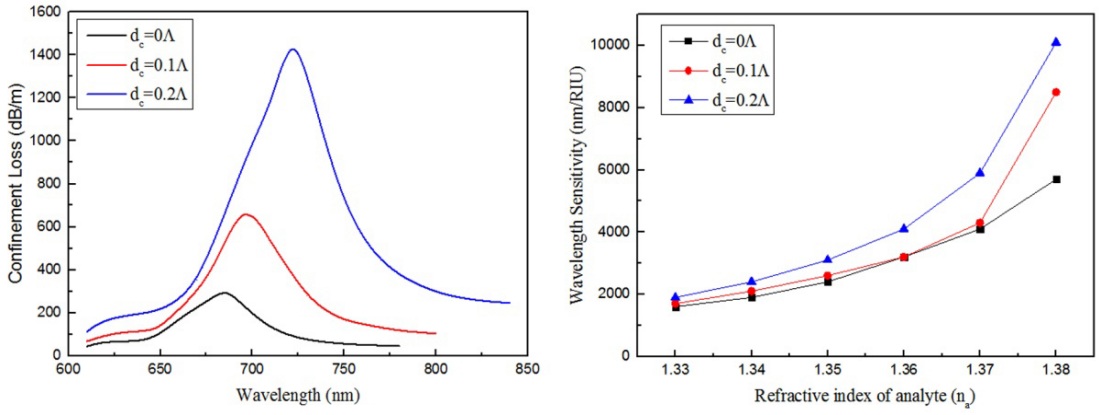

(a) (b)

FIG. 5. (a) Confinement loss of the core-guided mode for various diameters of the central hole with $n_a = 1.37$; (b) Wavelength sensitivities of the designed sensor with the diameter of the central hole when n_a changes from 1.33 to 1.39.

and the central air hole diameter is 0Λ, 0.1Λ, 0.2Λ, respectively. With the increasing of the d_c, the resonance intensity increases gradually, and the red shift occurs. This is due to the gradual increase in the size of d_c, which promotes the light leak from the core, resulting in the existence of a larger mode field near the metal interface, thereby enhancing the SPR phenomenon and resulting in higher propagation loss. Furthermore, the effective RI of the core-guided mode decreases with the increasing of the d_c, and the effective RI of the SPP mode is unchanged, so the phase matching point moves to the longer wavelength direction. The wavelength sensitivity varies with the diameter of central hole as shown in Fig. 5(b). It can be seen that the wavelength sensitivity increases gradually with the increase of RI. The wavelength sensitivity at different d_c for $n_a = 1.38$ is 5700 nm/RIU, 8500 nm/RIU and 10100 nm/RIU, respectively. However, when the diameter of d_c is further increased to 0.3Λ, the loss value is very large and energy cannot be well confined to the core. Especially, for high-RI samples, the sensing detection cannot be achieved in this case due to a decrease in the mode coupling efficiency.

The vertical distance (h) between the D-shaped hole and the core has a great influence on the performance of the sensor. As shown in Fig. 6, when the RI of analyte (n_a) is 1.37, the resonance intensity decreases and the formant has a redshift with h increasing from 2.6 μm to 3.0 μm. Due to the increase in distance, the gold-coating planes of the D-shaped holes are far from the air holes, which promotes the effective RI of the SPP mode increases, yet the effective RI of the core-guided mode is unchanged. So, the phase matching point moves in the longer wavelength direction. As the distance increases, the coupling efficiency between the core-guided mode and the SPP mode will decrease, resulting in lower sensitivity. However, the impact of the latter is much smaller than that of the former, so the trends in sensitivity variation are consistent with wavelength change.

Deviation in the manufacturing process may deteriorate the performance of the sensor. The influence of the deviation

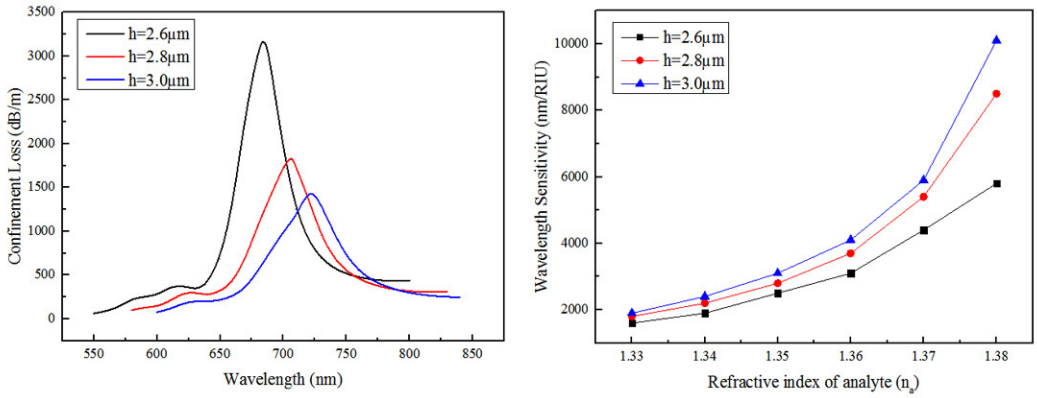

(a) (b)

FIG. 6. (a) The variation of loss with the distance between the D-shaped hole and the center of the fiber under the condition of $n_a = 1.37$; (b) The relationship between the RI of the analyte and the sensitivity at different distances.

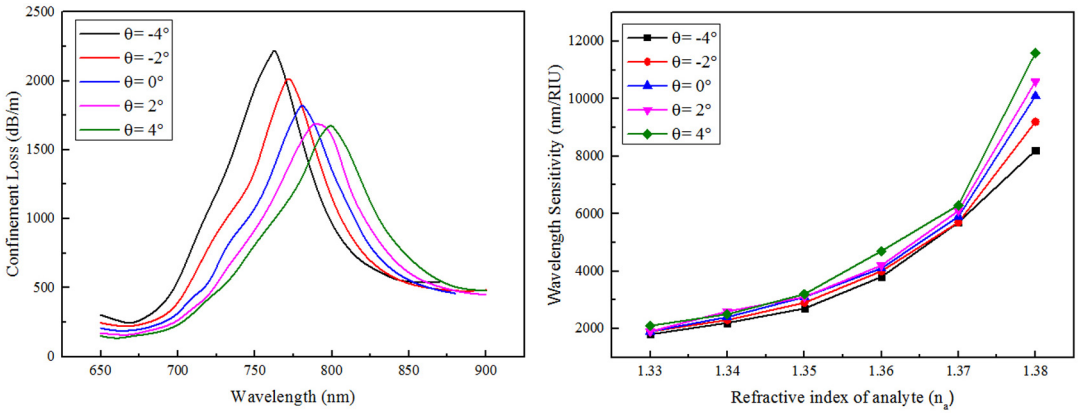

(a) (b)

FIG. 7. (a) The variation of the resonance peak with the deflection angle of the D-shaped holes for $n_a = 1.38$; (b) The relationship between the RI of the analyte and the sensitivity at different angles of rotation.

caused by the counterclockwise rotation of the D-shaped hole on the sensor is analyzed. The confinement loss is shown in Fig. 7(a), when the RI of analyte (n_a) is 1.38, and three D-shaped holes at a, b, c points are rotated counter-clockwise -4°, -2°, 0°, 2°, 4°, respectively. It can be seen that the resonance intensity gradually decreases and a red shift occurs as the angle of rotation gradually increases. This phenomenon can be explained by the principle of distance variation mentioned above. As the rotation angle (θ) increases, the average distance from the core increases, resulting in a decrease in resonance intensity. According to Fig. 7(b), the wavelength sensitivity of the sensor increases with the increase of the rotation angle due to the deviation caused by the counterclockwise rotation of the D-shaped holes at the time of fiber manufacturing.

IV. CONCLUSION

The characteristics of a novel PCF sensor with three D-shaped holes are numerically simulated in this paper. The design of D-shaped holes can be expanded outward until the planes of D-shaped holes are exposed in the air, solving the uniformity problem of metal nano-coating, and benefiting the filling of the analyte, so that the real-time detection of the analyte can be realized. Compared with the hexagonal arrangement, the triangular arrangement of the clad air holes can significantly reduce the transmission loss of light and improve the sensitivity of the sensor. The simulation results show that the dynamic detection range of the analyte is from 1.33 to 1.39, and the wavelength sensitivity can reach 10100 nm/RIU, the resolution is 9.9×10^{-6} RIU. In addition, the diameter of the air hole in the center of the PCF, the change of the distance between the D-shaped holes and the core, and the influence of the counterclockwise rotation angle of the D-shaped holes on the sensing performance are analyzed. The results show that higher wavelength sensitivity can be obtained with a larger diameter of the central air hole, the increasing distance between the D-shaped holes and the core leads to the red shift of the resonance peak. The deviation caused by the counterclockwise rotation of the D-shaped holes causes the wavelength sensitivity to increase with the increase of the rotation angle.

ACKNOWLEDGMENT

This research was funded by the National Natural Science Foundation of China (No. 61601183, 61675147) and the Graduate Education Innovation Program Fund of North China University of Water Resources and Electric Power (No. YK2018-12).

REFERENCES

1. A. Hassani and M. Skorobogatiy, "Design criteria for microstructured-optical-fiber-based surface-plasmon-resonance sensors," J. Opt. Soc. Am. B **24**, 1423-1429 (2007).
2. M. H. Chiu, M. H. Chi, and C. H. Shih, "Optimum sensitivities of D-type optical fiber sensor at a specific incident angle," Appl. Phys. A: Mater. Sci. Process. **89**, 413-416 (2007).
3. Y. Wang, J. Dostalek, and W. Knoll, "Magnetic nanoparticle-enhanced biosensor based on grating-coupled surface plasmon resonance," Anal. Chem. **83**, 6202-6207 (2011).
4. M. Tian, P. Lu, L. Chen, C. Lv, and D. Liu, "All-solid D-shaped photonic fiber sensor based on surface plasmon resonance," Opt. Commun. **285**, 1550-1554 (2012).
5. B. Li, M. Wu, X. Liu, G. Zhou, T. Wang, Z. Sheng, Z. Hou, and C. Xia, "Design and characterization of bio-chemical sensor based on photonic crystal fiber with fluorine-doped tin oxides film," Plasmonics **14**, 197-203 (2019).
6. M. S. Islam, J. Sultana, A. A. Rifat, R. Ahmed, A. Dinovitser, B. W.-H. Ng, H. Ebendorff-Heidepriem, and D. Abbott, "Dual-polarized highly sensitive plasmonic sensor in the visible to near-IR spectrum," Opt. Express **26**, 30347-30361 (2018).
7. X. Yang, Y. Lu, M. Wang, and J. Yao, "SPR sensor based on exposed-core grapefruit fiber with bimetallic structure," IEEE Photon. Technol. Lett. **28**, 649-652 (2016).
8. B. Shuai, L. Xia, Y. Zhang, and D. Liu, "A multi-core holey fiber based plasmonic sensor with large detection range and high linearity," Opt. Express **20**, 5974-5986 (2012).
9. Q. Liu, S. Li, and X. Gao, "Highly sensitive plasmonics temperature sensor based on photonic crystal fiber with a liquid core," Opt. Commun. **427**, 622-627 (2018).
10. P. Bing, S. Huang, J. Sui, H. Wang, and Z. Wang, "Analysis and improvement of a dual-core photonic crystal fiber sensor," Sensors **18**, 2051 (2018).
11. Z. Zhang, S. Li, Q. Liu, X. Feng, S. Zhang, Y. Wang, and J. Wu, "Groove micro-structure optical fiber refractive index sensor with nanoscale gold film based on surface plasmon resonance," Opt. Fiber Technol. **43**, 45-48 (2018).
12. X. Chen, L. Xia, and C. Li, "Surface plasmon resonance sensor based on a novel D-Shaped photonic crystal fiber for low refractive index detection," IEEE Photon. J. **10**, 1-9 (2018).
13. H. Fu, M. Zhang, J. Ding, J. Wu, Y. Zhu, H. Li, Q. Wang, and C. Yang, "A high sensitivity D-type surface plasmon resonance optical fiber refractive index sensor with graphene coated silver nano-columns," Opt. Fiber Technol. **48**, 34-39 (2019).
14. C. Liu, W. Su, Q. Liu, X. Lu, F. Wang, T. Sun, and P. K. Chu, "Symmetrical dual D-shape photonic crystal fibers for surface plasmon resonance sensing," Opt. Express **26**, 9039-9049 (2018).
15. X. Yang, Y. Lu, M. Wang, and J. Yao, "SPR sensor based on exposed-core grapefruit fiber with bimetallic structure," IEEE Photon. Technol. Lett. **28**, 649-652 (2016).
16. J. N. Dash and R. Jha, "Graphene-based birefringent photonic crystal fiber sensor using surface plasmon resonance," IEEE Photon. Technol. Lett. **26**, 1092-1095 (2014).
17. X. Yu, Y. Zhang, S. Pan, P. Shum, M. Yan, Y. Leviatan,

and C. Li, "A selectively coated photonic crystal fiber based surface plasmon resonance sensor," J. Opt. **12**, 015005 (2009).
18. C. Liu, F. Wang, J. Lv, T. Sun, Q. Liu, C. Fu, H. Mu, and P. K. Chu, "A highly temperature-sensitive photonic crystal fiber based on surface plasmon resonance," Opt. Commun. **359**, 378-382 (2016).
19. Q. Liu, S. Li, C. Dou, and X. Wang, "Defected-core photonic crystal fiber magnetic field sensor based on Sagnac interferometer," Appl. Phys. B: Lasers Opt. **123**, 65 (2017).
20. N. Luan and J. Yao, "Refractive index and temperature sensing based on surface plasmon resonance and directional resonance coupling in a PCF," IEEE Photon. J. **9**, 1-7 (2017).
21. R. K. Gangwar and V. K. Singh, "Highly sensitive surface plasmon resonance based D-shaped photonic crystal fiber refractive index sensor," Plasmonics **12**, 1367-1372 (2017).
22. J. Wu, S. Li, X. Wang, M. Shi, X. Feng, and Y. Liu, "Ultrahigh sensitivity refractive index sensor of a D-shaped PCF based on surface plasmon resonance," Appl. Opt. **57**, 4002-4007 (2018).
23. C. Liu, W. Su, F. Wang, X. Li, L. Yang, T. Sun, H. Mu, and P. K. Chu, "Theoretical assessment of a highly sensitive photonic crystal fibre based on surface plasmon resonance sensor operating in the near-infrared wavelength," J. Mod. Opt. **66**, 1-6 (2018).
24. P. Uebel, M. C. Günendi, M. H. Frosz, G. Ahmed, N. N. Edavalath, J. M. Ménard, and P. S. J. Russell, "Broadband robustly single-mode hollow-core PCF by resonant filtering of higher-order modes," Opt. Lett. **41**, 1961-1964 (2016).